

Article

Environment-Friendly Nanoporous Titanium Dioxide with Enhanced Photocatalytic Activity

Fatimah Al Qarni ¹, Nuhad A. Alomair ^{2,3} and Hanan H. Mohamed ^{2,3,*} 

¹ Department of Chemistry, Science College, Hafr Al Batin University, P.O. Box 1803, Hafr Al Batin 31991, Saudi Arabia; faelagame9@gmail.com

² Department of Chemistry, Science College, Imam Abdulrahman Bin Faisal University, P.O. Box 1982, Dammam 31441, Saudi Arabia; nalomair@iau.edu.sa

³ Basic and Applied Research Centre, Imam Abdulrahman Bin Faisal University, P.O. Box 1982, Dammam 31441, Saudi Arabia

* Correspondence: hhbesisa@iau.edu.sa

Received: 24 August 2019; Accepted: 18 September 2019; Published: 25 September 2019



Abstract: Nanoporous TiO₂ anatase was environment-friendly prepared using coffee husk extract (CHE) as bio-template instead of hazardous chemicals and solvents and ultrasonic waves. Caffeine and caffeic acid were found to be the main compounds in CHE to modify the morphology of TiO₂. The properties of as-prepared titanium dioxide particles were determined by different characterization techniques. The results demonstrate the formation of a meso/macro-porous channel consisting of small TiO₂ particles (8–10 nm). The as prepared green nanoparticles exhibited improved photocatalytic activity for the degradation of organic water pollutants with good recyclability. The enhancement in efficiency of green nanoporous TiO₂ can be attributed to higher surface area and the presence of more active adsorption sites inside the pores. The current research provides for a low cost, safe, and eco-friendly way to produce efficient photocatalysts for remediation of polluted water.

Keywords: nanoporous TiO₂ anatase; CHE; photocatalysis; methylene blue; phenol; antimicrobial agent; *E-Coli*

1. Introduction

Nowadays, water pollution has turned into a worldwide issue and the entire environment is aggravating as well as more diseases are caused worldwide due to water pollution [1,2]. Accordingly, water is treated in a number of traditional ways such as chemical precipitation, ion exchange, and electrochemical removal. But these procedures have huge drawbacks, as they lead to incomplete removal, require high-energy, and produce toxic materials [3–6]. Among various wastewater treatment methods, the photocatalytic process in aqueous suspension of semiconductor nanomaterials has received considerable attention in view of rapid and efficient destruction of pollutants [7–11]. Among various semiconductor nanomaterials, titanium dioxide (TiO₂) has been a widely investigated semiconductor as the most suitable material for environmental and energy applications due to its unique properties [12]. There are many ways for the preparation of TiO₂ such as the solvothermal method, hydrothermal method, sol-gel method, chemical vapor deposition, and electrodeposition. Nevertheless, these methods require high energy and hazardous materials and solvents [13–16]. Green synthesis of nanomaterials is an alternative route to physical and chemical methods that leads to environment-friendly products due to the use of non-toxic materials, and does not require high temperatures and pressure, and at a lower cost. Green synthesis may be by microorganisms, plant extracts, and plant biomass [17,18]. Therefore, using such a green and environmentally friendly method can also minimize the use of chemicals and toxic solvents. In order

to control crystal growth, approaches including the use of plant extracts as reducing/oxidizing agents, stabilizers, and capping agent, have been carried out [16,17]. Chemical compounds in the plant extract play the role of bio-template producing nanomaterials with modified morphology [17]. In addition, the eco-friendly method for synthesis of nanomaterials can also be achieved by reducing the required process temperature, using microwave or ultrasonic waves [7–18]. In recent years a number of nanoparticles have been prepared using fungi, bacteria, actinomycetes, and enzymes [19–23] and also have been used as many plant extracts such as camellia sinensis, neem, coriandrum, ocimum sanctum, nelumbo lucifera [24–26]. Recently, researchers have been able to achieve the biosynthesis of nanoparticles by any part of the plant parts such as leg, leaves, roots, flowers, buds, and seeds [27]. The use of plants to produce nanoparticles has drawn attention more than the use of other biological processes as less costly, faster, non-pathogenic, and safer [28]. Due to the variety of plants, we can easily change the source of the extract and thus control the morphology and the size of the nanoparticles as needed [29]. Plant extracts are usually stable even following multi months and do not demonstrate any noticeable changes [30]. The principle phytochemicals responsible for the synthesis of nanoparticles are alkaloids, tannins, phenolic, flavones, ketones, aldehydes, terpenoids, amides, and carboxylic acid [31–35].

The present paper reports the results of an ongoing study on the preparation of modified titanium dioxide nanomaterials using the environment-friendly method. In this study, the chemical compounds in the plant waste, particularly coffee husk, have been exploited as bio-template to produce nanoporous TiO₂ with small particle size. The as prepared green nanoporous TiO₂ exhibited enhanced photocatalytic activity under UV and solar light irradiation as compared to their counterparts prepared in the absence of the plant waste extract. Hence, this study provides the simple and green method to produce porous TiO₂ nanoparticles with enhanced activity for water remediation.

2. Results and Discussion

2.1. Characterization

2.1.1. Characterization of Coffee Husk Extract

CHE was analyzed by UV-vis absorption and FTIR spectra (see Figure 1a,b, respectively). UV-vis absorption spectroscopy measurement of CHE with absorption in the range 200–400 nm shows two peaks, one peak at 275 nm attributed to caffeine and the peak at 320 nm attributed to caffeic acid [36,37]. The results indicate the presence of polyphenolic, caffeic acid and caffeine which act as bio-template forming porous TiO₂ nanoparticles.

FTIR spectrum of the as obtained CHE show broad absorption peak from 3600 to 3200 cm⁻¹ which can be assigned to –OH in polyphenolic compounds in CHE. The carbonyl C=O stretching vibration appears at 1700 cm⁻¹ in infrared spectrum of the free caffeine. A peak occurs at 1655 cm⁻¹ of (C=O) and (C=C) in free caffeine [38]. The quadratal CN stretching in imidazole ring appears at 1403 cm⁻¹ of the caffeine. The vibrations of free caffeine appear at 2900, 1700, 1683, 1456 and the broad bands at 1284–973, 925 cm⁻¹.

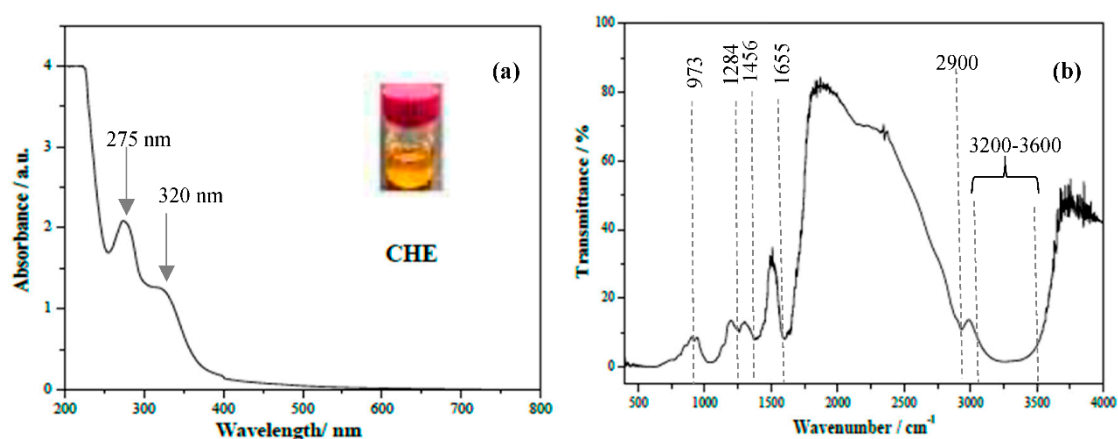


Figure 1. (a) UV-vis spectrum and (b) FTIR of the coffee husk extract (CHE).

2.1.2. Characterization of TiO₂ Nanomaterials

Figure 2 shows the XRD patterns of chemically as well as green prepared TiO₂ nanoparticles. XRD of both TiO₂ samples shows the diffractions peaks at 25.28°, 37.93°, 48.37°, 53.89°, 55.29°, 62.73°, 69.00°, and 75.37° for anatase phase (JCPDS no. 21-1272) [39]. Moreover, the intensities diffraction peak decreases and becomes broader for green TiO₂ nanoparticles indicating smaller particle size [40]. The crystallite size of the as prepared TiO₂ nanomaterials has been determined from the XRD data using the Scherrer equation to be 16 and 7.5 nm respectively, for chemically as well as green prepared TiO₂ nanoparticles, respectively.

The morphological features of chemically as well as green prepared TiO₂ nanoparticles have been determined by SEM and TEM measurements. SEM images TiO₂ sample prepared in presence and in absence of CHE are Figure 3a–c. It was found that, while agglomeration of TiO₂ particles was observed for the TiO₂ sample prepared without CHE (Figure 3a), the macro porous structure with pore size of range 1.3–1.6 μm was observed for the TiO₂ sample prepared with CHE (Figure 3b,c). The diameter of the TiO₂ particles was noticed to be smaller for green TiO₂ nanoparticles (8–10 nm) (Figure 4b) as compared to chemically prepared TiO₂ (Figure 4a). The TEM results were found to be in good agreement with the XRD measurements.

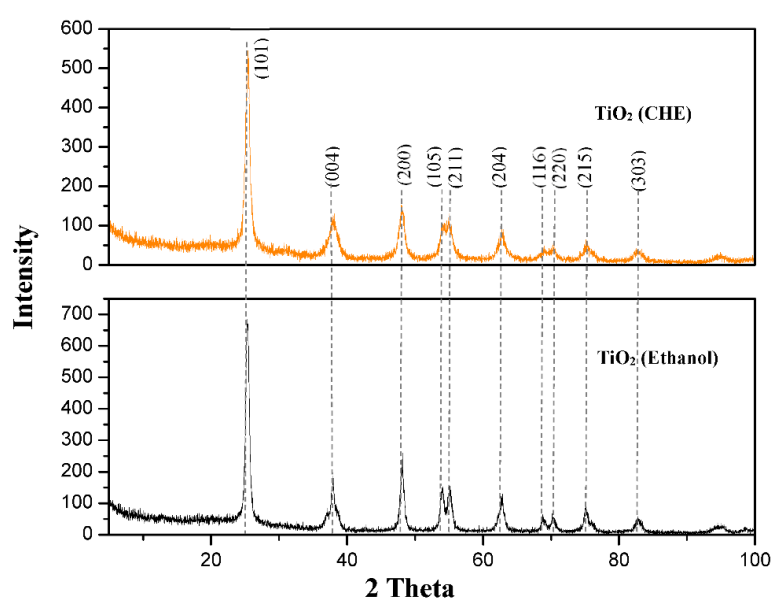


Figure 2. XRD patterns of the as synthesized nanomaterials.

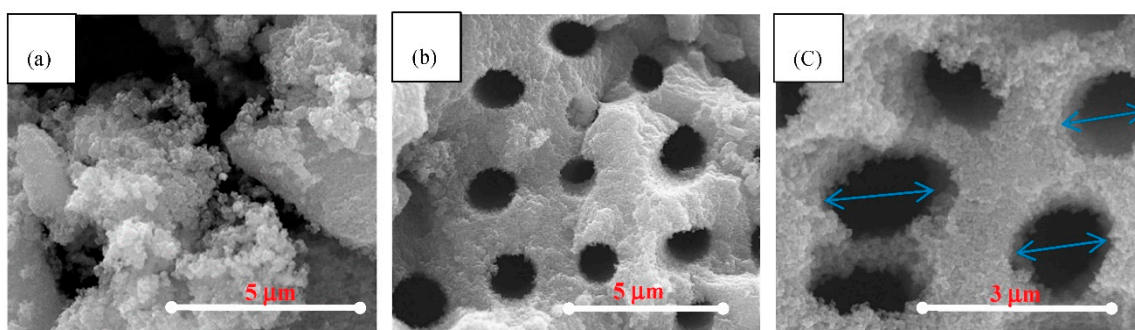


Figure 3. SEM micrographs of the as synthesized TiO₂ nanomaterials prepared without CHE (a) and with CHE (b,c).

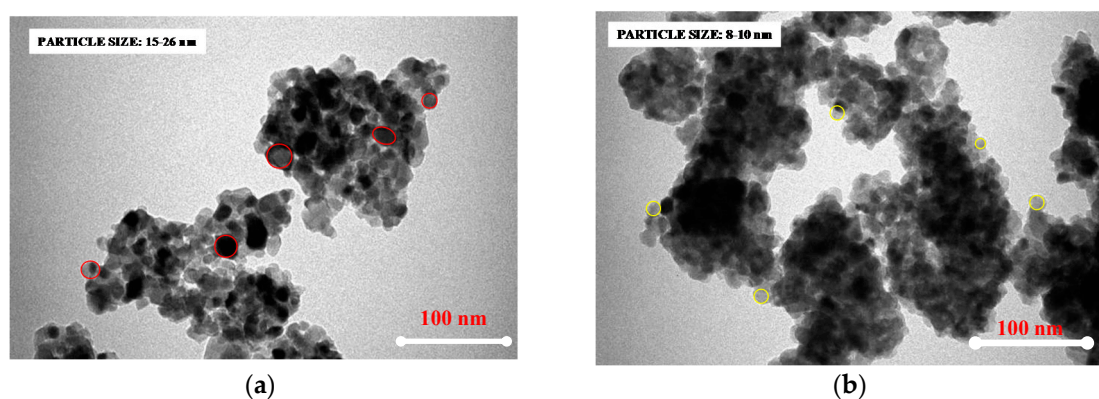


Figure 4. TEM micrographs of the as synthesized TiO₂ nanomaterials prepared without CHE (a) and with CHE (b).

Figure 5a,b shows the Raman and FTIR spectra of the as synthesized nanomaterials. The Raman spectra of the TiO₂ samples prepared with and without CHE show the characteristic peaks of pure anatase phase. The band at 390 cm⁻¹ is assigned to *B1g*. The bands at 510 and 620 cm⁻¹ are assigned to *A1g* and the band at 140 cm⁻¹ is assigned to *Eg*, which are all related to the anatase phase [41]. As shown in the inset of Figure 7a, no apparent peaks of carbon have been observed, confirming that, carbon did not dope into the TiO₂ lattice in both TiO₂ samples. The FTIR spectrum of TiO₂ nanomaterials prepared with and without CHE present similar FTIR spectra with peak around 450 cm⁻¹ assigned to stretching vibration of Ti–O–Ti bonds. The broad band at 3428 cm⁻¹ can be ascribed to the –OH stretching vibration of the adsorbed water molecules on TiO₂ surface and the peak around 1630 cm⁻¹ is attributed to the bending vibrations of –OH [42]. The FTIR results indicated no adsorption of the plant extract compounds on TiO₂ surface after calcination at 773 K.

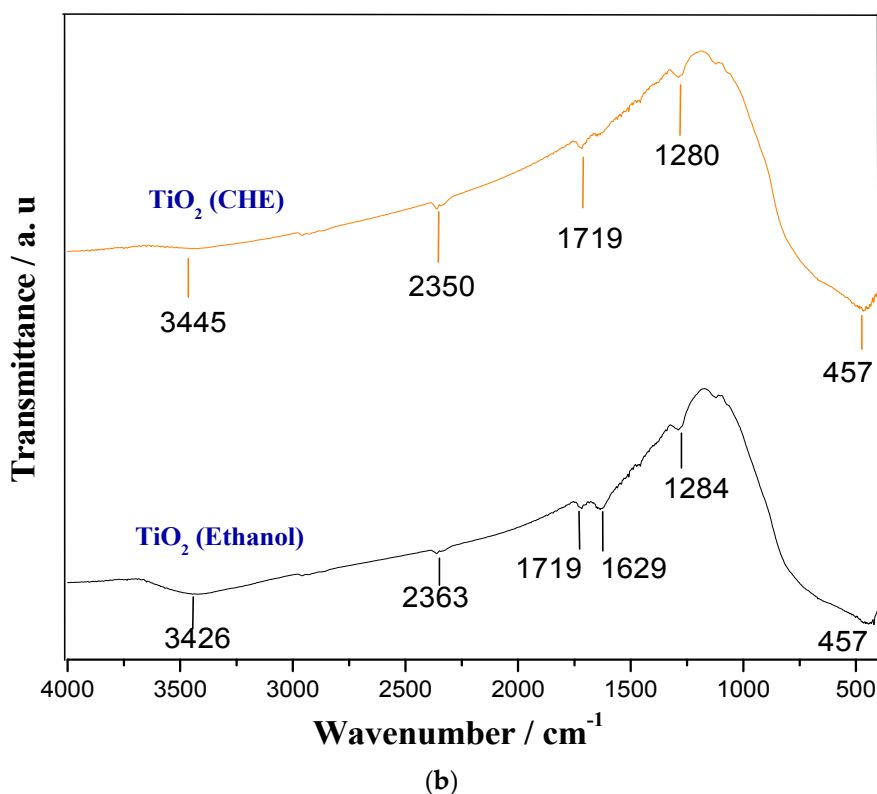
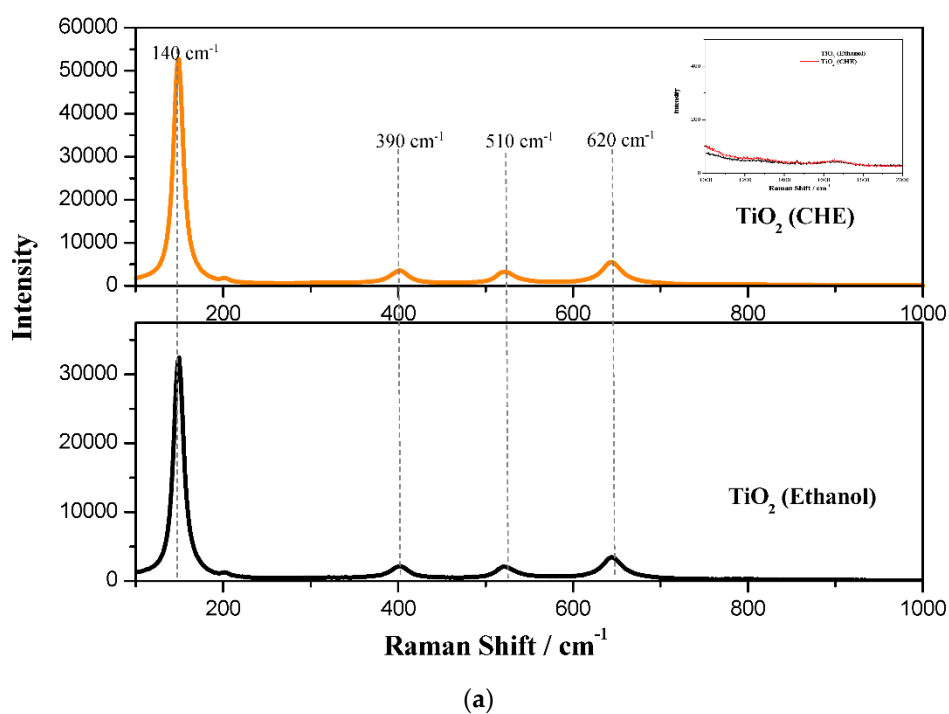
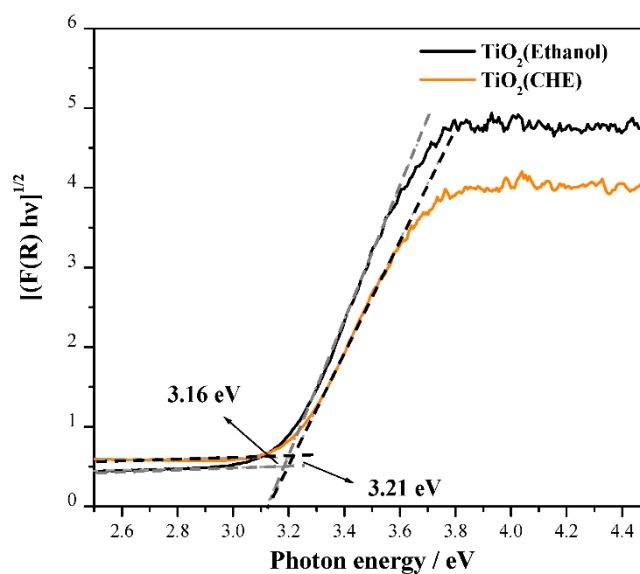


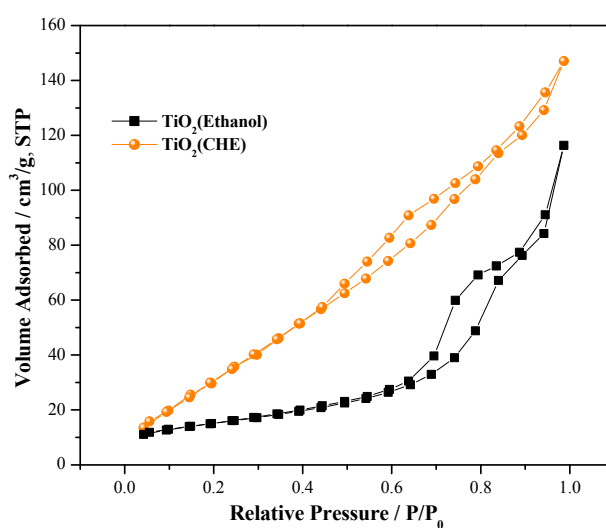
Figure 5. Raman spectra (a) and FTIR spectra (b) of the as synthesized TiO₂ nanomaterials. The inset of (a) shows the enlargement for the area of carbon.

The UV-vis diffuse reflectance measurements (Figure 6a) show that both TiO₂ samples can only absorb UV light and reflect most light in the visible region. The band gap energy has been estimated using the Kubelka–Munk relation [43]. The band gap energy of nanomaterials prepared with and without CHS was estimated to be 3.21 eV and 3.16 eV, respectively. A slight increase in the band gap energy of the TiO₂ sample prepared with CHE was observed which can be attributed to the

smaller particle size [44]. Figure 6b shows the N₂ adsorption–desorption measurements of the samples. The adsorption–desorption isotherms of both samples can be assigned to typical H3 hysteresis loop. The BET surface area of the samples revealed that TiO₂ prepared with CHE exhibited larger surface area of about 147.15 m²/g compared to TiO₂ nanoparticles prepared without CHE (53.96 m²/g) (Table 1), which can be readily attributed to the porous structure as well as the small particle size of the green TiO₂ particles prepared with CHE.



(a)



(b)

Figure 6. UV-vis diffuse reflectance spectra of the as synthesized TiO₂ nanomaterials (a), N₂ adsorption-desorption isotherms of the as synthesized nanomaterials (b).

Table 1. The surface area and the porous parameters of the as prepared nanomaterials.

Nanomaterial	BET (m ² /g)	Pore Volume (cc/g)	Pore Size (nm)
TiO ₂ (Ethanol)	53.96	2.49×10^{-2}	9.24×10^2
TiO ₂ (CHE)	147.15	5.54×10^{-2}	7.53×10^2

2.2. Photocatalytic Performance

Photocatalytic performance of the as prepared nanomaterials has been evaluated for the degradation MB dye. The change in MB concentration was determined from UV-vis absorbance measurements. The absorbance of MB with λ_{\max} 668 nm was found to decrease gradually with irradiation (Figure 7a,b).

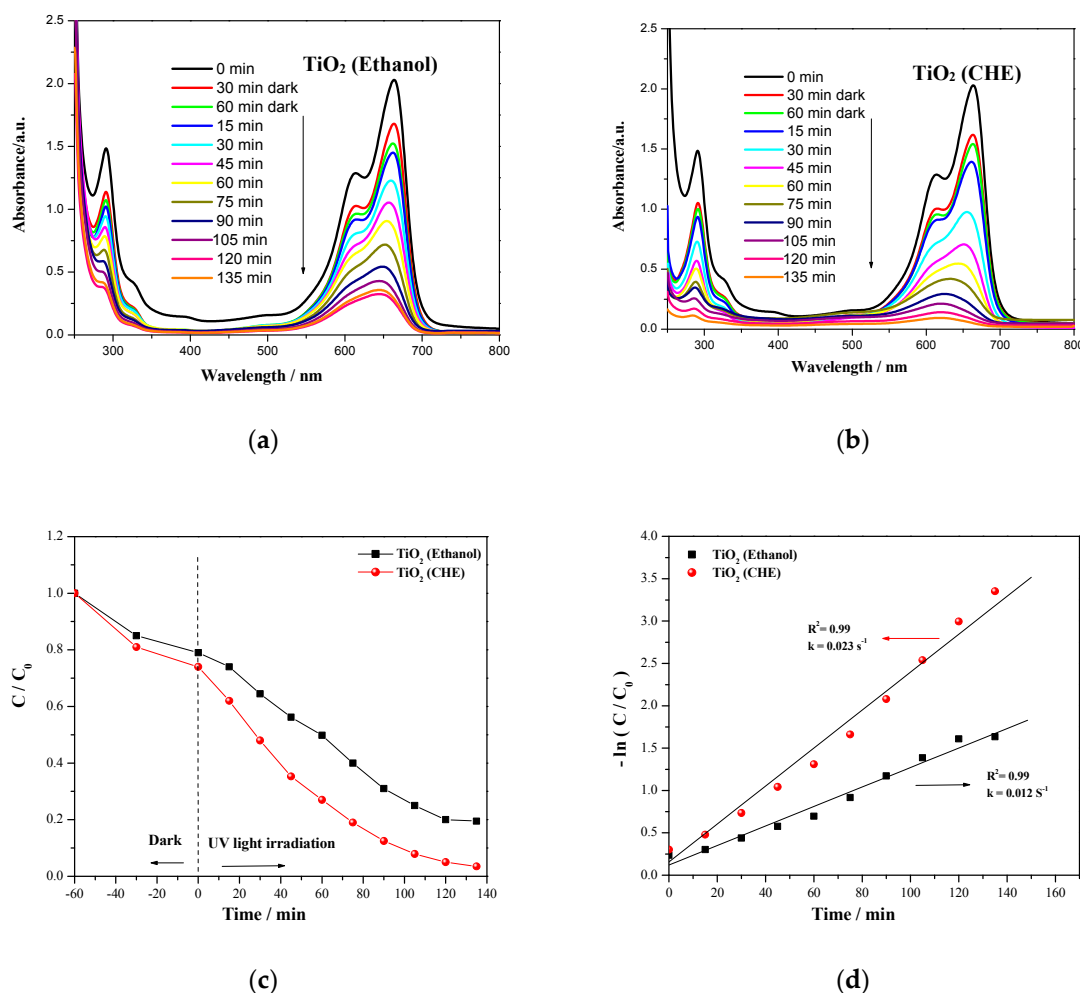


Figure 7. (a,b) UV-vis absorption spectra of an aqueous solution of MB during solar light illumination in the presence of the as synthesized TiO₂ (ethanol) and TiO₂ (CHE), respectively; (c) efficiency of the photocatalytic degradation of MB as the variation of C/C_0 with irradiation time in the presence of various nanomaterials; (d) linear plots of $-\ln(C/C_0)$ vs. time for the experimental data in Figure 7c.

The photocatalytic degradation efficiency for MB degradation is shown in Figure 7c. Slow degradation was shown when TiO₂ (ethanol) nanomaterial is used as a catalyst, while more efficient degradation was obtained in presence of TiO₂ (CHE).

Since phenol frequently exists in industry effluents and is difficult to be degraded due to the stability of the benzene ring, the photocatalytic degradation of phenol was of interest. The degradation of phenol was monitored using the UV-vis absorbance measurement in the wavelength range (200–400 nm) (Figure 8a,b) with two characteristic bands at 210 nm and 269 nm. Upon irradiation in the presence of TiO₂ nanoparticles, a gradual decrease in intensity of phenol absorbance was observed, confirming the decrease in phenol concentration. Figure 8c shows the photocatalytic degradation efficiency for phenol degradation using various TiO₂ nanomaterials. Noticeable photocatalytic improvement has been achieved when TiO₂ (CHE) was used as the catalyst.

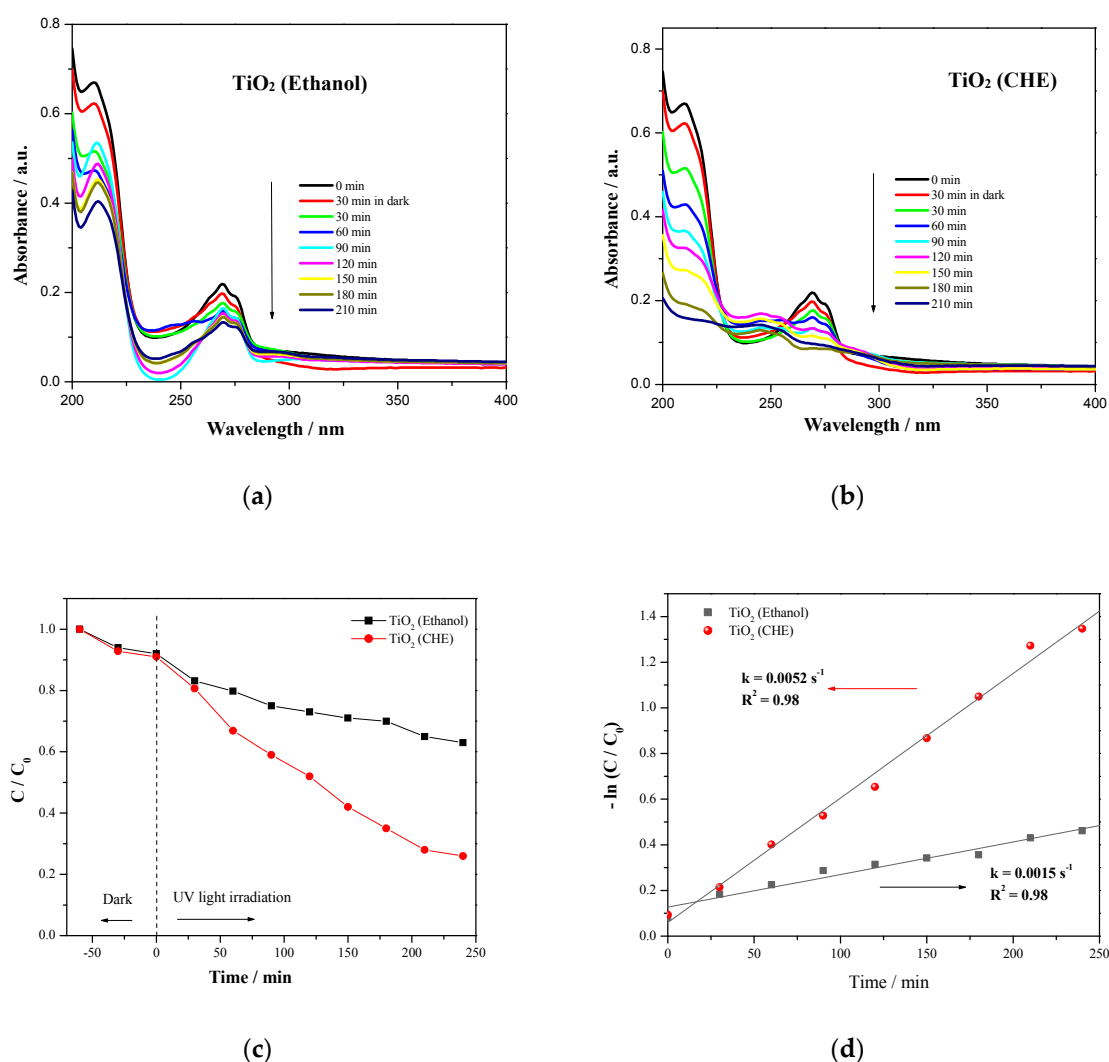


Figure 8. (a,b) UV-vis absorption spectra of an aqueous solution of phenol during solar light illumination in the presence of the as synthesized TiO_2 (Ethanol) and TiO_2 (CHE), respectively; (c) efficiency of the photocatalytic degradation of MB as the variation of C/C_0 with irradiation time in the presence of various nanomaterials; (d) linear plots of $-\ln(C/C_0)$ vs. time for the experimental data in Figure 8c.

The kinetics of MB and phenol degradation have been also investigated by plotting $-\ln(C/C_0)$ with time. Linear correlation for MB and phenol degradation was obtained for all samples which fit well with the pseudo first-order model (Figures 7d and 8d, respectively) and the apparent rate constant k' (min^{-1}) has been estimated and the data have been gathered in Table 2. It was found that, the observed rate constant of photocatalytic degradation of MB in the presence of TiO_2 (CHE) is around 2 times higher than that in the presence of TiO_2 (ethanol). In addition, the photocatalytic degradation of phenol in the presence of TiO_2 (CHE) is three times higher than that when used TiO_2 (ethanol) (Table 2).

Table 2. Kinetic parameters obtained from first order fitting the experimental points of Figures 7 and 8.

Nanomaterial	Reactant	k' (min^{-1})	R^2
TiO_2 (Ethanol)	MB	0.012	0.99
TiO_2 (Ethanol)	Phenol	0.0015	0.97
TiO_2 (CHE)	MB	0.023	0.99
TiO_2 (CHE)	Phenol	0.0052	0.99

The improvement of the photocatalytic performance of TiO₂ (CHE) can be attributed to increasing the surface area as well as the active adsorption sites inside the pores, leading to increased accessibility for the organic pollutant and therefore enhancing photocatalytic performance.

The recyclability of the green TiO₂ has been studied for 3 cycles of photocatalytic degradation of MB (20 mg L⁻¹). Ninety-eight percent of MB was degraded even after the 3rd cycle, indicating the stability and recyclability of green nanoporous TiO₂ photocatalyst (Figure 9).

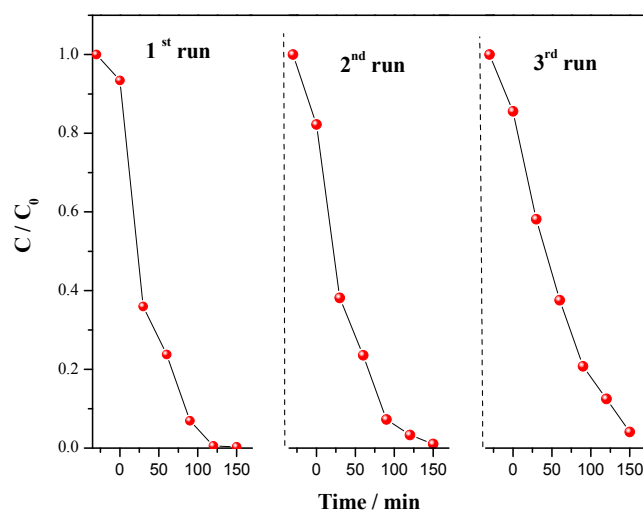


Figure 9. Recyclability of the as prepared green TiO₂ in the photocatalytic degradation of MB.

3. Experimental

3.1. Preparation of Coffee Husk Extract

Coffee husk of Arabian coffee obtained from the western province, Saudi Arabia were washed several times with distilled water to remove the dust particles on their surface then dried in air. The dried husk was grinded to obtain fine powder. Twenty (20) g of coffee husk was boiled with 400 mL of distilled water for 30 min, then allowed to cool down slightly and finally filtered to obtain a clear brown solution of coffee husk extract (CHE) (Figure 10). It can be kept in a dark bottle in the fridge for further use.

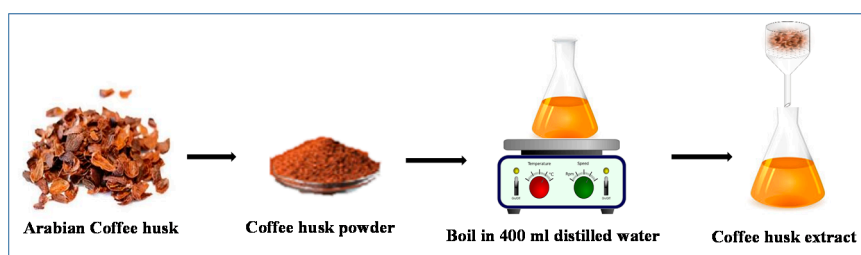


Figure 10. Schematic representation of preparation of coffee husk extract (CHE).

3.2. Synthesis of TiO₂ Nanoparticles Using CHE

Two hundred (200) mL of the CHE solution was placed in a conical flask. Five (5) mL of titanium tetraisopropoxide (TTIP) was drop-wise added to the CHE solution under ultrasonic waves. The obtained suspension was stirred overnight. After that, solid TiO₂ nanoparticles were separated and washed 3 times by centrifuge. Then, dried in the oven at 70 °C and finally calcined at 500 °C for 1 h (Figure 11). For comparison, TiO₂ nanoparticles were prepared in absence of CHE, in typical synthesis, 5 mL of (TTIP) in 15 mL ethanol was drop-wise added to ethanol/water solution (1:1) under continuous

stirring for overnight. The TiO₂ nanoparticles were separated and washed 3 times by centrifuge and denoted as (TiO₂ ethanol).

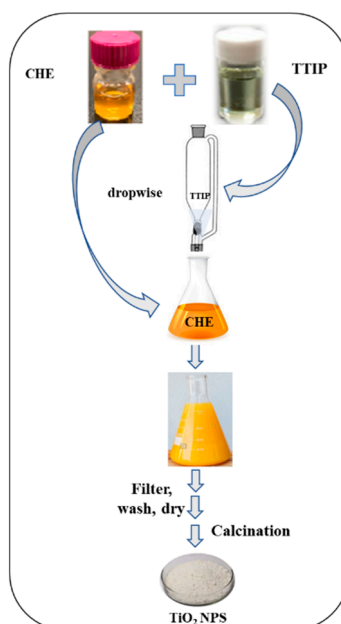


Figure 11. Schematic representation of preparation of porous TiO₂ nanoparticles.

3.3. Characterization

XRD measurements were performed using Shimadzu's-XRD Powder diffractometer (xrd-700, Maxima, Shimadzu, Kyoto, Japan) with a Cu radiation source, at a scanning speed of 2 min⁻¹, 40 kV tube voltage, and 30 mA tube current. FTIR measurements were recorded on IR AFFINITY-1 Shimadzu (Shimadzu, Kyoto, Japan) by Fourier transform and KBr (Potassium Bromide) pellets were used to obtain the absorption spectra in infrared region for the CHE as well as nanomaterials. Raman spectroscopy was conducted on iHR320 with CCD detector, HORIBA at 632 nm excitation wavelength, DXR Raman Microscope, DXR 532 nm Laser. SEM images were taken using Hitachi S-4700 (Hitachi, Žatec, Czech Republic) using the following parameters: acceleration voltage = 20 kV, working distance about 10 mm and spot size 3. The powder specimens were mounted onto a metallic stub with a double-sided adhesive tape. Images were captured at different magnifications. For transmission electron microscopy (TEM), the powder was dispersed in ethanol, sonicated for 5 min and deposited onto TEM grid having carbon support film. The grids were dried before mounting into the TEM. A TEM, FEI, Morgagni, Cze Republic at 80 kV was used to record the images. The UV-vis diffuse reflectance measurements were performed on Shimadzu UV4100 spectrometer (Shimadzu, Kyoto, Japan) and UV-vis absorption measurements were recorded on UV-vis Spectrophotometer-UVD-3200 (LABOMED, Los Angeles, CA, USA).

3.4. Photocatalytic Activity

The photocatalytic performance of the green as well as chemically synthesized TiO₂ nanoparticles has been evaluated for photocatalytic degradation of methylene blue (MB) as model pollutant under solar light irradiation. The photocatalytic activity was further evaluated for the photocatalytic mineralization of phenol under solar light irradiation. The photocatalytic experiments were carried out using solar simulator (SLB-300A, 300 W). The amount of the degraded organic pollutant (MB or phenol) was evaluated from UV-vis spectroscopic measurement before and during illumination.

4. Conclusions

Nanoporous TiO₂ has been synthesized using plant waste extract (CHE). The properties of produced green nanomaterials were well determined using diverse characterization techniques. SEM and TEM analysis revealed that the produced green nanomaterials have macroporous/mesoporous structures composed of small-sized TiO₂ particles and narrow particle distribution. The as synthesized green porous TiO₂ nanomaterials showed enhanced photocatalytic performance under UV and solar light irradiation for degradation of organic dyes and phenol. The enhanced photocatalytic activity of the green TiO₂ can be attributed to higher surface area and the presence of more active adsorption sites inside the pores leading to increased accessibility for the organic pollutant and therefore enhancing photocatalytic activity. The results demonstrate the efficiency of CHE as bio-template to produce porous TiO₂ nanoparticles with enhanced photocatalytic activity.

Author Contributions: Conceptualization, H.H.M.; Methodology, H.H.M.; Validation, F.A.Q., N.A.A. and H.H.M.; Formal Analysis, F.A.Q. and H.H.M.; Investigation, F.A.Q. and H.H.M.; Data Curation, F.A.Q. and H.H.M.; Writing-Original Draft Preparation, H.H.M. and F.A.Q.; Writing-Review & Editing, H.H.M.; Supervision, H.H.M. and N.A.A.

Funding: This research received no external funding.

Acknowledgments: The authors acknowledge Imam Abdulrahman Bin Faisal University for supporting this work. The authors acknowledge Institution of Research and Medical Consultations (IRMC) for SEM and TEM measurements. Department of Chemistry-College of Science-King Fahd University of Petroleum and Minerals is gratefully acknowledged for Raman measurements.

Conflicts of Interest: The authors declare that they have no competing interests.

References

1. Chaudhry, F.N.; Malik, M.F. Factors Affecting Water Pollution: A Review. *J. Ecosyst. Ecography* **2017**, *7*, 6–8.
2. Site, A.D. Factors affecting sorption of organic compounds in natural sorbent/water systems and sorption coefficients for selected pollutants. A review. *J. Phys. Chem. Ref. Data* **2001**, *30*, 187–439. [[CrossRef](#)]
3. Eccles, H. Treatment of metal-contaminated wastes: Why select a biological process? *Trends Biotechnol.* **1999**, *17*, 462–465. [[CrossRef](#)]
4. Muller-Karger, F.E.; McClain, C.R.; Richardson, P.L. The dispersal of the Amazon's water. *Nature* **1988**, *333*, 56–59. [[CrossRef](#)]
5. Schalscha, B.E.; Ahumada, T.I. Heavy metals in rivers and soils of central Chile. *Water Sci. Technol.* **1998**, *37*, 251–255. [[CrossRef](#)]
6. Fu, F.; Wang, Q. Removal of heavy metal ions from wastewaters: A review. *J. Environ. Manag.* **2011**, *92*, 407–418. [[CrossRef](#)]
7. Mohamed, H.H. Sonochemical synthesis of ZnO hollow microstructure/reduced graphene oxide for enhanced sunlight photocatalytic degradation of organic pollutants. *J. Photochem. Photobiol. A* **2018**, *353*, 401–408. [[CrossRef](#)]
8. Mohamed, H.H.; Alomair, N.A.; Bahnemann, D.W. Kinetic and mechanistic features on the reaction of stored TiO₂ electrons with Hg (II), Pb (II) and Ni (II) in aqueous suspension. *Arab. J. Chem.* **2016**, in press. [[CrossRef](#)]
9. Mohamed, H.H. Rationally designed Fe₂O₃/GO/WO₃ Z-Scheme photocatalyst for enhanced solar light photocatalytic water remediation. *J. Photochem. Photobiol. A* **2019**, *378*, 74–84. [[CrossRef](#)]
10. Mohamed, H.H.; Alsanea, A.A.; Alomair, N.A.; Akhtar, S.; Bahnemann, D.W. ZnO@ porous graphite nanocomposite from waste for superior photocatalytic activity. *Environ. Sci. Pollut. Res.* **2019**, *26*, 12288–12301. [[CrossRef](#)]
11. Mohamed, H.H.; Alsanea, A.A. TiO₂/Carbon Dots Decorated Reduced Graphene Oxide Composites from Waste Car Bumper and TiO₂ Nanoparticles for Photocatalytic Applications. *Arab. J. Chem.* **2018**, in press. [[CrossRef](#)]
12. Mohamed, H.H.; Dillert, R.; Bahnemann, D.W. TiO₂ nanoparticles as electron pools: Single- and multi-step electron transfer processes. *J. Photochem. Photobiol. A Chem.* **2012**, *245*, 9–17. [[CrossRef](#)]
13. Su, C.; Hong, B.-Y.; Tseng, C.-M. Sol-gel preparation and photocatalysis of titanium dioxide. *Catal. Today* **2004**, *96*, 119–126. [[CrossRef](#)]

14. Lakshmi, B.B.; Patrissi, C.J.; Martin, C.R. Sol–Gel Template Synthesis of Semiconductor Oxide Micro- and Nanostructures. *Chem. Mater.* **1997**, *9*, 2544–2550. [[CrossRef](#)]
15. Chen, X.; Mao, S.S. Titanium dioxide nanomaterials: Synthesis, properties, modifications and applications. *Chem. Rev.* **2007**, *107*, 2891–2959. [[CrossRef](#)] [[PubMed](#)]
16. Youssef, T.E.; Mohamed, H.H. Synthesis and photophysical properties of novel mononuclear rhodium(III) phthalocyanines. *Polyhedron* **2011**, *30*, 2045–2050. [[CrossRef](#)]
17. Alomair, N.; Mohamed, H.H.; Alomair, N. Green synthesis of ZnO hollow microspheres and ZnO/rGO nanocomposite using red rice husk extract and their photocatalytic performance. *Mater. Res. Express* **2018**, *5*, 095012. [[CrossRef](#)]
18. Mohamed, H.H.; Alomair, N.A.; Akhtar, S.; Youssef, T.E. Eco-friendly synthesized α -Fe₂O₃/TiO₂ heterojunction with enhanced visible light photocatalytic activity. *J. Photochem. Photobiol. A Chem.* **2019**, *382*, 111951. [[CrossRef](#)]
19. Ahmed, S.; Ahmad, M.; Swami, B.L.; Ikram, S. A review on plants extract mediated synthesis of silver nanoparticles for antimicrobial applications: A green expertise. *J. Adv. Res.* **2016**, *7*, 17–28. [[CrossRef](#)]
20. Hunagund, S.M.; Desai, V.R.; Barretto, D.A.; Pujar, M.S.; Kadadevarmath, J.S.; Vootla, S.; Sidarai, A.H. Photocatalysis effect of a novel green synthesis gadolinium doped titanium dioxide nanoparticles on their biological activities. *J. Photochem. Photobiol. A Chem.* **2017**, *346*, 159–167. [[CrossRef](#)]
21. Saravanan, M.; Gopinath, V.; Chaurasia, M.K.; Syed, A.; Ameen, F.; Purushothaman, N. Green synthesis of anisotropic zinc oxide nanoparticles with antibacterial and cytofriendly properties. *Microb. Pathog.* **2018**, *115*, 57–63. [[CrossRef](#)]
22. Mohamed, H.H.; Hammami, I.; Baghdadi, H.A.; Al-Jameel, S.S. Multifunctional TiO₂ microspheres-rGO as highly active visible light photocatalyst and antimicrobial agent. *Mater. Express* **2018**, *8*, 345–352. [[CrossRef](#)]
23. Lengke, M.; Southam, G. Bioaccumulation of gold by sulfate-reducing bacteria cultured in the presence of gold(I)-thiosulfate complex. *Geochim. Cosmochim. Acta* **2006**, *70*, 3646–3661. [[CrossRef](#)]
24. Mukherjee, P.; Ahmad, A.; Mandal, D.; Senapati, S.; Sainkar, S.R.; Khan, M.I.; Parishcha, R.; Ajaykumar, P.V.; Alam, M.; Kumar, R.; et al. Fungus-Mediated Synthesis of Silver Nanoparticles and Their Immobilization in the Mycelial Matrix: A Novel Biological Approach to Nanoparticle Synthesis. *Nano Lett.* **2001**, *1*, 515–519. [[CrossRef](#)]
25. Holmes, J.D.; Smith, P.R.; Richardson, D.J.; Russell, D.A.; Sodeau, J.R. Energy-dispersive X-ray analysis of the extracellular cadmium sulfide crystallites of *Klebsiella aerogenes*. *Arch. Microbiol.* **1995**, *163*, 143–147. [[CrossRef](#)] [[PubMed](#)]
26. Willner, I.; Basnar, B.; Willner, B. Nanoparticle-enzyme hybrid systems for nanobiotechnology. *FEBS J.* **2007**, *274*, 302–309. [[CrossRef](#)]
27. Begum, N.A.; Mondal, S.; Basu, S.; Laskar, R.A.; Mandal, D. Biogenic synthesis of Au and Ag nanoparticles using aqueous solutions of Black Tea leaf extracts. *Colloids Surf. B Biointerfaces* **2009**, *71*, 113–118. [[CrossRef](#)]
28. Philip, D. Biosynthesis of Au, Ag and Au-Ag nanoparticles using edible mushroom extract. *Spectrochim. Acta Part A Mol. Biomol. Spectrosc.* **2009**, *73*, 374–381. [[CrossRef](#)]
29. Narayanan, K.B.; Sakthivel, N. Coriander leaf mediated biosynthesis of gold nanoparticles. *Mater. Lett.* **2008**, *62*, 4588–4590. [[CrossRef](#)]
30. Husen, A.; Siddiqi, K.S. Phytosynthesis of nanoparticles: Concept, controversy and application. *Nanoscale Res. Lett.* **2014**, *9*, 229. [[CrossRef](#)]
31. Shankar, S.; Rai, A.; Ahmad, A.; Sastry, M. Rapid synthesis of Au, Ag, and bimetallic Au core–Ag shell nanoparticles using Neem (*Azadirachta indica*) leaf broth. *J. Colloid Interface Sci.* **2004**, *275*, 496–502. [[CrossRef](#)] [[PubMed](#)]
32. Shukla, R.C.; Tandon, P.K.; Singh, S.B. Removal of Arsenic(III) from Water with Clay-Supported Zerovalent Iron Nanoparticles Synthesized with the Help of Tea Liquor. *Ind. Eng. Chem. Res.* **2013**, *52*, 10052–10058.
33. Huang, L.; Weng, X.; Chen, Z.; Megharaj, M.; Naidu, R. Synthesis of iron-based nanoparticles using oolong tea extract for the degradation of malachite green. *Spectrochim. Acta Part A Mol. Biomol. Spectrosc.* **2014**, *117*, 801–804. [[CrossRef](#)] [[PubMed](#)]
34. Roopan, S.M.; Bharathi, A.; Prabhakarn, A.; Rahuman, A.A.; Velayutham, K.; Rajakumar, G.; Padmaja, R.D.; Lekshmi, M.; Madhumitha, G. Efficient phyto-synthesis and structural characterization of rutile TiO₂ nanoparticles using *Annona squamosa* peel extract. *Spectrochim. Acta Part A Mol. Biomol. Spectrosc.* **2012**, *98*, 86–90. [[CrossRef](#)] [[PubMed](#)]

35. Sundrarajan, M.; Gowri, S. Green synthesis of titanium dioxide nanoparticles by nyctanthes arbor-tristis leaves extract. *Chalcogenide Lett.* **2011**, *8*, 447–451.
36. Souto, U.T.D.C.P.; Barbosa, M.F.; Dantas, H.V.; de Pontes, A.S.; da Silva Lyra, W.; Diniz, P.H.G.D.; Araújo, M.C.U.; da Silva, E.C. Identification of adulteration in ground roasted coffees using UV-Vis spectroscopy and SPA-LDA. *LWT Food Sci. Technol.* **2015**, *63*, 1037–1041.
37. Suhandy, D.; Yulia, M. Peaberry coffee discrimination using UV-visible spectroscopy combined with SIMCA and PLS-DA. *Int. J. Food Prop.* **2017**, *20* (Supp. 1), S331–S339. [[CrossRef](#)]
38. Srivastava, S.K.; Singh, V.B. Ab initio and DFT studies of the structure and vibrational spectra of anhydrous caffeine. *Spectrochim. Acta Part A Mol. Biomol. Spectrosc.* **2013**, *115*, 45–50. [[CrossRef](#)]
39. Sutradhar, P.; Saha, M.; Maiti, D. Microwave synthesis of copper oxide nanoparticles using tea leaf and coffee powder extracts and its antibacterial activity. *J. Nanostruct. Chem.* **2014**, *4*, 4–9. [[CrossRef](#)]
40. Sharma, R.; Bisen, D.P.; Shukla, U.; Sharma, B.G. X-ray diffraction: A powerful method of characterizing nanomaterials. *Recent Res. Sci. Technol.* **2012**, *4*, 77–79.
41. Ohsaka, T.; Izumi, F.; Fujiki, Y. Raman spectrum of anatase, TiO₂. *J. Raman Spectrosc.* **1978**, *7*, 321–324. [[CrossRef](#)]
42. Mohamed, H.H. Biphasic TiO₂ microspheres/reduced graphene oxide for effective simultaneous photocatalytic reduction and oxidation processes. *Appl. Catal. A Gen.* **2017**, *541*, 25–34. [[CrossRef](#)]
43. López, R.; Gómez, R. Band-gap energy estimation from diffuse reflectance measurements on sol-gel and commercial TiO₂: A comparative study. *J. Sol Gel Sci. Technol.* **2012**, *61*, 1. [[CrossRef](#)]
44. Singh, M.; Goyal, M.; Devlal, K. Size and shape effects on the band gap of semiconductor compound nanomaterials. *J. Taibah Univ. Sci.* **2018**, *12*, 470–475. [[CrossRef](#)]



© 2019 by the authors. Licensee MDPI, Basel, Switzerland. This article is an open access article distributed under the terms and conditions of the Creative Commons Attribution (CC BY) license (<http://creativecommons.org/licenses/by/4.0/>).